International Symposium on Earthquake Engineering, JAEE, Vol.2, 2013

DETECTION OF THREE-DIMENSIONAL CRUSTAL MOVEMENTS DUE TO THE 2011 TOHOKU EARTHQUAKE FROM SAR IMAGES

Wen LIU[1], Fumio YAMAZAKI[2], Takashi NONAKA[3] and Tadashi SASAGAWA[3]

[1] Post-doctoral research fellow, Interdisciplinary Graduate School of Science and Engineering, Tokyo Institute of Technology, Tokyo, Japan, liu.w.ad@m.titech.ac.jp
[2] Professor, Graduate School of Engineering, Chiba University
Chiba, Japan, yamazaki@tu.chiba-u.ac.jp
[3] Satellite Business Division, PASCO Corporation, Tokyo, Japan
taakka9299@pasco.co.jp; taawda5004@pasco.co.jp

ABSTRACT: A method for capturing the two-dimensional (2D) surface movements from two temporal TerraSAR-X (TSX) intensity images has been proposed by the authors in the previous research. In this study, three pairs of TSX images taken in ascending and descending paths were used to estimate 3D crustal movements by the proposed method. First, the 2D crustal movements were detected from the three sets respectively. Then the absolute 3D movements were estimated by the combination of the detected 2D movements. The results were verified by the GEONET observation records.

Key Words: pixel-offset, building, TerraSAR-X images

INTRODUCTION

The Mw 9.0 Tohoku Earthquake occurred on March 11, 2011, off the Pacific coast of northeastern (Tohoku) Japan, caused gigantic tsunamis, resulting in widespread devastation. According to the GPS Earth Observation Network System (GEONET) at the Geospatial Information Authority (GSI) in Japan, crustal movements with maximums of 5.3 m to the horizontal (southeast) and 1.2 m to the vertical (downward) directions were observed over a wide area (Ozawa *et al.*, 2011). The high-accuracy georeferenced product has become available recently due to the improvement of SAR sensors, and thus an improved pixel-offset method was proposed by the present authors to estimate the absolute ground displacements in case of large-scale tectonic movements (Liu and Yamazaki, 2013). The three-dimensional (3D) actual displacement is converted into two-dimensional (2D) one when taken by a SAR sensor, due to its side-looking observing model. From one pair of SAR images, only the converted 2D displacement can be detected. However, if there are at least two sets of 2D results, the 3D displacement can be estimated using the parameters of shooting conditions.

The 3D surface displacement estimates have been obtained by both InSAR and pixel-offset methods using SAR data pairs captured from ascending and descending orbits (Fialko *et al.*, 2001; Tobita *et al.*, 2006). Minet et. al (2011) obtained 3D-motion vectors to describe the surface displacement caused by the 2010 Haiti earthquake from several ascending- and descending-paths

TerraSAR-X (TSX) images. Matsuoka and Kodamo (2011) recently measured the coseismic displacement due to the 2010 EI Mayor, Mexico earthquake from the pre- and post-event orthorectified ASTER/PRISM mosaic images. In this study, three pairs of pre- and post-event TSX intensity images from the 2011 Tohoku earthquake taken in different paths were used to detect the 2D displacements by the proposed method. Then the 3D displacement was estimated from the three sets of detected results from different pre- and post-event pairs by a regression analysis. Finally, the accuracy of 3D estimation was examined by comparing the detected displacements and those from GPS ground station records.

STUDY AREA AND IMAGE DATA

The study area was focused on the coastal zone of Tohoku, Japan, as shown in Fig. 1, which was one of the most severely affected areas in the 2011 Tohoku earthquake. Three pairs TSX images taken before and after the earthquake were used for detecting crustal movements. The common part enclosed by the black frame is the target area. The first pair was taken in the ascending path, with a pre-event image on October 9, 2009 (Local time) and a post-event one on April 1, 2011. The incident angle is 35.23° at the center of the images and the heading angle is 349.79° clockwise from the north. The two other pairs were taken in the descending path. The second pair includes a pre-event image on October 26, 2010 and a post-event one on March 29, 2011. The incident angle is 21.47° at the center of the images and the heading angle is 191.32°. The third pair includes a pre-event image on October 21, 2010 and a post-event one on April 4, 2011. The incident angle at the center is 37.31° and the heading angle is 190.03°.

All the pairs were taken by HH polarization in the StripMap mode. The azimuth and range resolutions were about 3 m. The images were provided as the Enhanced Ellipsoid Corrected (EEC) products. Two preprocessing approaches were applied before detecting crustal movements. First, the two TSX intensity images were transformed to a Sigma Naught (σ^0) value, which represents the radar reflectivity per unit area in the ground range. An Enhanced Lee filter (Lopes *et al.*, 1990) was then applied to the original SAR images to reduce the speckle noise. To minimize any loss of information included in the intensity images, the window size of the filter was set as 3 × 3 pixels. The pixel localization corrected by the GPS orbit determination was used directly in this study. According to the product specification document (Eineder *et al.*, 2010), the pixel localization accuracy of the EEC products depends on the orbit and the DEM used. Since the orbit type of our TSX images was "Science", their required orbit accuracy is within 20 cm, but actual data showed better than 10 cm accuracy (Wermuth *et al.*, 2009). Three GPS stations of GEONET, “Rifu”, “Natori” and “Watari”, exist in the target area. The color composites of the pre- and post-event images from the three pairs are shown in Fig. 2.

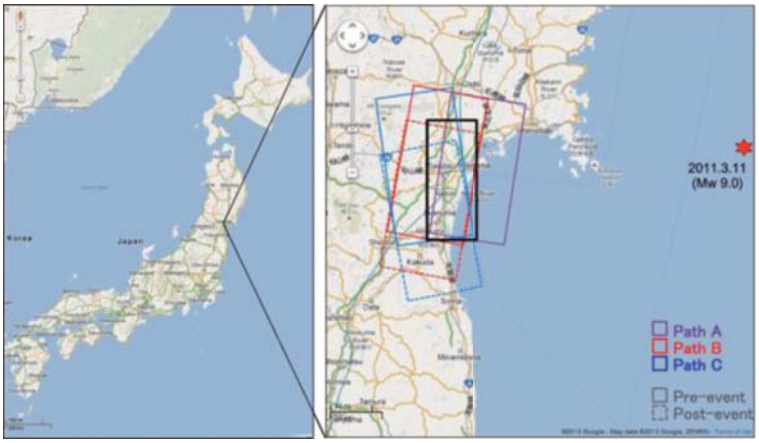

Fig. 1 Study area with six TerraSAR-X images in Miyagi Prefecture.

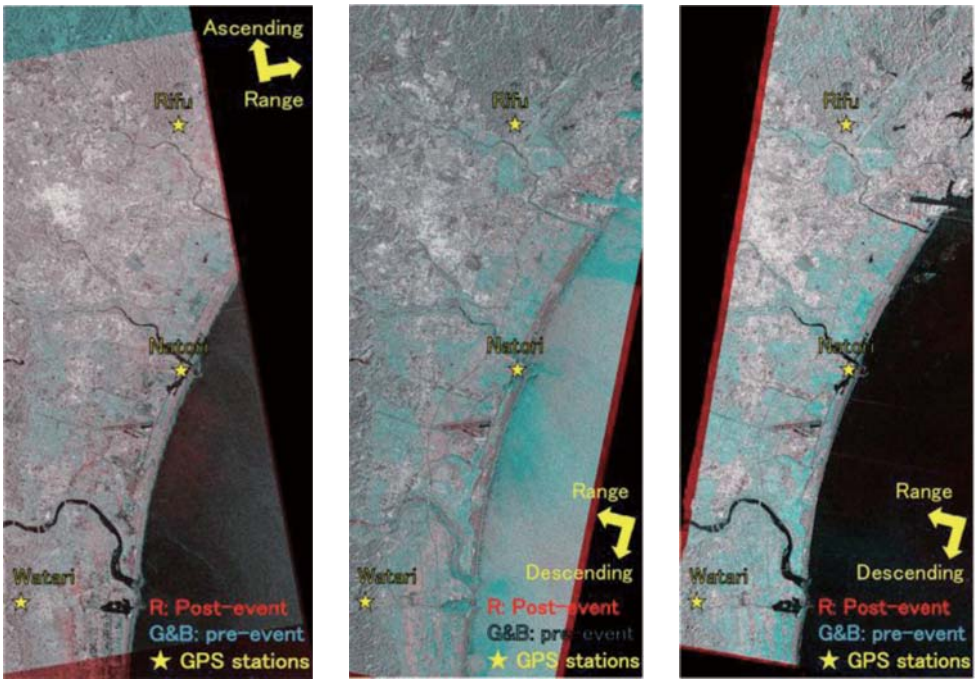

(a) Path A (b) Path B (c) Path C

Fig. 2 Color composites of the three pairs of pre- and post-event TSX images in Paths A (a), B (b), and C (c), with three GPS ground control stations.

DETECTION OF TWO-DIMENSIONAL CRUSTAL MOVEMENT

The crustal movements within the target area were extracted by the proposed pixel-offset method (Liu and Yamazaki, 2013). Firstly, the whole target area was divided into a 2.5 × 2.5 km^2 mesh. In each sub-area, solid buildings larger than 150 m^2 were extracted by a simple segmentation approach. Then the non-changed buildings were extracted by comparing the building locations in the two images. If a solid building exists in the post-event image around the location of a target building in the pre-event image within 5 pixels, the target building is regarded as non-changed. The displacement of a non-changed building between the two TSX intensity images was calculated by an area correlation method. To improve the accuracy, the TSX images surrounding non-changed structures were resampled to 0.25 m/pixel by cubic convolution to have 1/5 of the original pixel size. Thus the shift of buildings could be detected at a sub-pixel level.

The crustal movements in the whole area were detected in the same way. Finally, the average value of these movements was calculated and considered as the crustal movement in that sub-area. To ensure the reliability of the results, only sub-areas containing more than 5 building displacements were counted as valid ones. The results of three pairs were obtained and shown in Fig. 3. The detected movements in the sub-areas including the GPS stations were shown in Table 1.

Table 1. Detected 2D displacements from three pairs in the sub-areas including Rifu, Natori, and Watari GPS stations (unit: meter).

Path	Rifu		Natori		Watari	
	East	North	East	North	East	North
Path *A*	3.44	-0.95	3.47	-0.66	3.11	-0.58
Path *B*	3.21	-0.69	2.69	-0.38	2.67	-0.67
Path *C*	3.48	-0.90	3.49	-0.68	2.28	-0.57

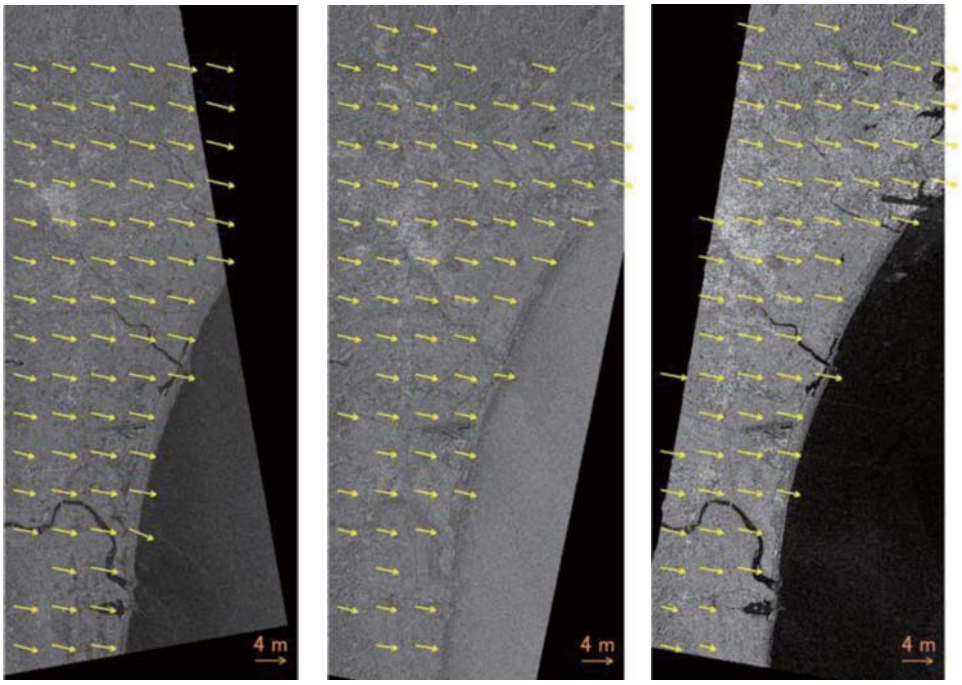

(a) Path A (b) Path B (c) Path C

Fig. 3 Detected displacement vector in each sub-area plotting on the pre-event TSX images from Paths A (a), B (b) and C (c), respectively.

ESTIMATION OF THREE-DIMENSIONAL DISPLACEMENTS

The surface displacement is a vector in the three-dimensional space with three components, D_E, D_N, and D_Z, to the east, north, and vertical directions, respectively. The proposed pixel-offset method can detect a 2D movement, in which the 3D movement is transformed to the east and north directions. The movement to the vertical direction is decomposed and transformed to the movements to the east and north directions. The relationship between an actual 3D crustal movement and its 2D shift in a ground range SAR image is represented by Eq. (1).

$$\begin{pmatrix} M_E \\ M_N \end{pmatrix} = \begin{pmatrix} 1 & 0 & -\cos\alpha / \tan\theta \\ 0 & 1 & \sin\alpha / \tan\theta \end{pmatrix} \begin{pmatrix} D_E \\ D_N \\ D_Z \end{pmatrix} \tag{1}$$

where D is the actual movement to the east, north, and vertical directions; M is the shift in the SAR image; α is the heading angle clockwise from the north; and θ is the SAR incident angle.

Detected 2D result from one pair of TSX images is not enough to estimate 3D movement. However, two pairs of different observation sets can build four individual equations, and then they make 3D estimation possible. Since the crustal movement before the 2011 Tohoku earthquake was approximately zero, the geo-locations of the three pre-event TSX images were almost the same. In addition, there were only 6 days differences between the three post-event images. According to the GPS records, the displacements during the first post-event image taken on March 29, 2011 and the last pre-event image taken on April 4, 2011 were very small. Thus, the crustal movements in the three pairs of the images can be regarded as the same. Then six equations can be built from the three pairs' results according to Eq. (1).

Since the number of equations is more than the number of the unknown displacements in the three directions, a regression analysis was applied to calculate the most suitable displacement values. From two sets of results, one 3D displacement can be estimated by regression using Eq. (2).

$$\begin{pmatrix} M_{Ea} \\ M_{Na} \\ M_{Eb} \\ M_{Nb} \end{pmatrix} = \begin{pmatrix} 1 \\ 0 \\ 1 \\ 0 \end{pmatrix} D_E + \begin{pmatrix} 0 \\ 1 \\ 0 \\ 1 \end{pmatrix} D_N + \begin{pmatrix} -\cos\alpha_a / \tan\theta_a \\ \sin\alpha_a / \tan\theta_a \\ -\cos\alpha_b / \tan\theta_b \\ \sin\alpha_b / \tan\theta_b \end{pmatrix} D_Z \quad (2)$$

where D is are independent variables (the actual geodetic movement to the east, north, and vertical directions) to obtain at a point; M_{ij}s are dependent variables (the shift in the SAR image to the east and north directions) obtained from the 2D analysis for the j-th pre- and post-event acquisition pair.

Three combinations exist using two pairs of results, one with ascending path A and descending path B, one with path A and descending path C, and one with paths B and C. The regression analysis was applied to all the combinations. The 3D displacement in each sub-area was estimated and shown in Fig. 4. The red vectors indicate movements to the horizontal direction and the blue vectors to the vertical direction. Since the vertical movements were much smaller than the horizontal ones, they are shown at a different scale.

The horizontal displacements from these combinations were similar and show stable results. The vertical displacements from the set using the ascending path A and descending path B were more stable than other two sets. The vertical displacements estimated from the descending paths B and C were significantly larger than that from the combinations of ascending and descending paths. The second set using the ascending path A and descending path C obtained the smallest vertical displacements. Many vertical displacements from this set were upward.

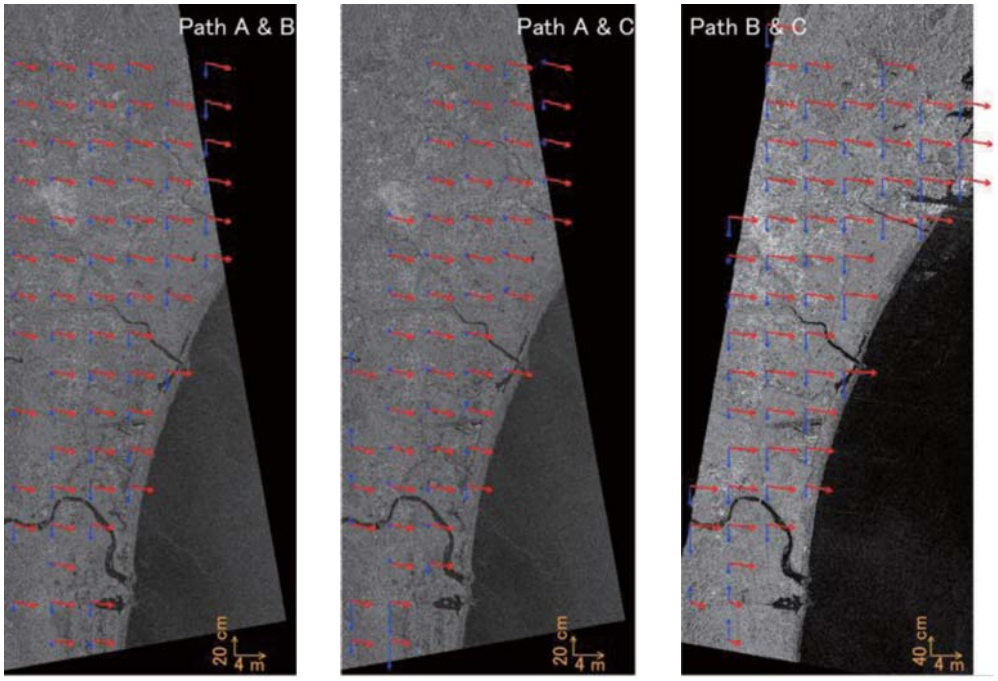

(a) (b) (c)

Fig. 4 Estimated displacement vectors in each sub-area overlapping on the pre-event TSX images from the pairs of Paths A and B (a), A and C (b), B and C (c), respectively.

The estimated results in the sub-areas including GPS ground stations using two sets of results are shown in Table 2, comparing with the GPS results. The Roo Mean Square (RMS) error was calculated in the three directions between the results and GPS records. The RMS errors for the first set were the smallest in the sub-area including the Rifu and Watari stations. The RMS error for the second set was the smallest in the sub-area including Natori station. In addition, the RMS errors for the third set were largest in all the sub-areas including GPS stations. It can be confirmed that the combinations using

ascending and descending paths have better results than that using only descending paths. In addition, the combinations using the pairs with the different looking angles (21° and 35°) have better results than that using the pairs with the similar looking angles (35° and 37°).

The estimation using three sets of results was also carried out by regression analysis using Eq. (3). Since not all sub-areas have results from all the three pairs, the sub-areas having results from at least two pairs were calculated. According to the comparisons shown in Table 2, the combinations with the ascending and descending paths had higher accuracy than that with the two descending paths. Thus, estimations from two pairs were obtained only for the first and second combinations.

$$\begin{pmatrix} M_{Ea} \\ M_{Na} \\ M_{Eb} \\ M_{Nb} \\ M_{Ec} \\ M_{Nc} \end{pmatrix} = \begin{pmatrix} 1 \\ 0 \\ 1 \\ 0 \\ 1 \\ 0 \end{pmatrix} D_E + \begin{pmatrix} 0 \\ 1 \\ 0 \\ 1 \\ 0 \\ 1 \end{pmatrix} D_N + \begin{pmatrix} -\cos\alpha_a / \tan\theta_a \\ \sin\alpha_a / \tan\theta_a \\ -\cos\alpha_b / \tan\theta_b \\ \sin\alpha_b / \tan\theta_b \\ -\cos\alpha_c / \tan\theta_c \\ \sin\alpha_c / \tan\theta_c \end{pmatrix} D_Z \tag{3}$$

The estimated result using three sets was shown in Fig. 5(a). The specific pairs used for the estimation in each sub-area are shown in Fig. 5(b). The displacement amplitudes to the horizontal and vertical directions are shown in Fig. 5(c) and (d), respectively, in rainbow color.

The 3D movements were detected for 73 sub-areas (approximately 456 km^2). The displacements of 52 sub-areas were estimated using the three sets of result. From Fig. 5(c-d), it can be confirmed that the largest movement occurred around the northeastern coast and the values became smaller going southwards. The detected movement increasingly points to the east direction as the location becomes more southerly. These trends matched the observed GEONET's GPS data (Ozawa *et al.*, 2011). The maximum subsidence also occurred along the coast and became smaller further westwards. This trend was also coincident with the observed GPS data. However, the detected results were unstable for several sub-areas. When comparing the estimated results with the number of used pairs, it could be confirmed that result in the sub-areas estimated from the three pairs was more stable than that estimated from only two pairs.

The comparison of the 3D results detected around the three GPS stations using three sets of results is also shown in Table 2. The average differences between our results and the GPS measurements were approximately 0.09 m in the horizontal and 0.13 m in the vertical directions. The RMS errors at the three sub-areas in the 3D space were all less than 0.15 m. Comparing with the estimated displacements using two sets of results, the RMS errors around Rifu and Watari stations are larger, however, the estimation using three sets can obtain more stable displacements.

Table 2. Comparison of the estimated 3D displacements from the three different pairs by the regression analysis with those from GPS records (unit: meter).

Path		A & B	A & C	B & C	3 pairs	GPS
Rifu	E	3.36	3.46	3.69	3.41	3.34
	N	-0.80	-0.93	-0.73	-0.83	-0.86
	Z	-0.06	0.01	-0.18	-0.04	-0.28
	RMS	0.13	0.19	0.22	0.15	
Natori	E	3.19	3.48	4.22	3.34	3.36
	N	-0.45	-0.67	-0.33	-0.52	-0.77
	Z	-0.20	0.01	-0.59	-0.16	-0.22
	RMS	0.21	0.16	0.60	0.15	
Watari	E	2.93	2.66	1.91	2.79	2.96
	N	-0.57	-0.48	-0.73	-0.55	-0.53
	Z	-0.11	-0.30	0.30	-0.14	-0.24
	RMS	0.08	0.18	0.69	0.11	

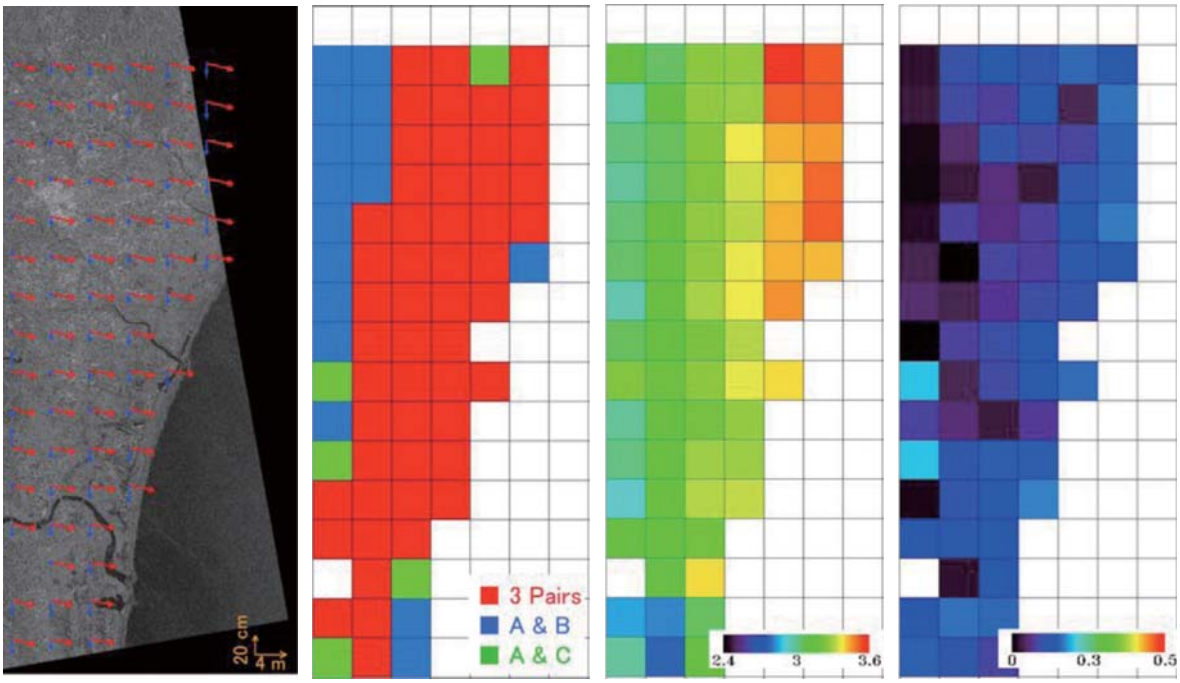

(a) (b) (c) (d)

Fig. 5 Estimated 3D displacement vector using three pairs (a) and the pairs used for the estimation (b); the displacement amplitude in the horizontal (c) and vertical (d) directions shown in rainbow color.

CONCLUSIONS

In this study, three-dimensional (3D) displacements due to the 2011 Tohoku, Japan, earthquake were estimated from three pairs of the pre- and post-event TSX images. Firstly, two-dimensional (2D) displacements were detected from each pair by an enhanced pixel-offset method. The common area for the three pairs of images was divided in to 2.5 km^2 meshes. 2D displacements were calculated in each sub-area. Then the three-dimensional displacements were estimated according to the relationship between the 2D observation of the sensor and the real 3D displacements. A regression analysis was applied to obtain the most suitable 3D displacements from the three pairs' 2D results by sub-area unit. The 3D displacements were estimated using two pairs' and three pairs' results, respectively. Comparing with the GPS ground station records, the error of the 3D estimation was less than 0.3 m, which is 1/10 of the original image resolution. The RMS error around Rifu and Watari GPS stations was smallest using the data taken from Path A and Path C, which had different incident angles and heading directions. The RMS error around Natori station was smallest using the three sets data. Although the results obtained in this study are promising, we will further test the proposed method for other events including smaller surface displacements to validate its applicability.

ACKNOWLEDGMENT

TerraSAR-X data was owned by German Aerospace Center (DLR) and provided by PASCO Corporation.

REFERENCES

Fialko, Y., Simons, M. and Agnew, D. (2001). "The complete (3-D) surface displacement field in the

epicentral area of the 1999 Mw. 7.1 Hector Mine earthquake California, from space geodetic observations." *Geophysical Research Letters*, Vol. 28 No. 16, 3063-3066.

Liu, W. and Yamazaki, F. (2013). "Detection of crustal movement from TerraSAR-X intensity image." *IEEE Geoscience and Remote sensing Letters*, Vol. 10, No. 1, 199–203.

Lopes, A., Touzi, R. and Nezy, E. (1990). "Adaptie speckle filters and scene heterogeneity." *IEEE Transactions on Geoscience and Remote Sensing*, Vol. 28, 992 -1000.

Matsuoka, M. and Kodama, S. (2011). "Coseismis displacement measurement of the 2010 EL Mayor Mexico Earthquake by subpixel correlation from optical satellite images." *IEEE IGARSS 2011*, Vancouver, 4010-4013.

Minet, C., Eineder, M. and Yague-Martines, N. (2011). "Haiti earthquake (12.01.2010) surface shift estimation using TerraSAR-X data." *IEEE IGARSS 2011*, Vancouver, 2488-2491.

Ozawa, S., Nishimura, T., Suito, H., Kobayashi, T., Tobita, M. and Imakiire, T. (2011). "Coseismic and postseismic slip of the 2011 magnitude-9 Tohoku-Oki earthquake." *Nature*, Vol. 475 No. 7356, 373–377.

Tobita, M., Suito, H., Imakiire, T., Kato, M., Fujiwara, S. and Murakami, M. (2006). "Outline of vertical displacement of the 2004 and 2005 Sumatra earthquakes revealed by satellite radar imagery." *Earth Planets Space*, Vol. 48, No. 1, e1–e4.

Wermuth, M., Hauschild, A., Montenbruck, O. and Jäggi, A. (2009). "TerraSAR-X Rapid and Precise Orbit Determination." *21st International Symposium on Space Flight Dynamics*, France.

Zebker, H.A. (2000). "Studying the Earth with interferometric radar." *IEEE Computing in Science & Engineering*, Vol. 2, No. 3, 52-60.

(Abstract Submitted: August 29, 2013)
(Accepted: September 13, 2013)